# Dynamic modulation of ANO1/TMEM16A $HCO_3^-$ permeability by $Ca^{2+}$/calmodulin

Jinsei Jung[a,b], Joo Hyun Nam[c], Hyun Woo Park[a], Uhtaek Oh[d], Joo-Heon Yoon[b], and Min Goo Lee[a,1]

[a]Department of Pharmacology, Brain Korea 21 Project for Medical Sciences, and [b]Department of Otorhinolaryngology, Yonsei University College of Medicine, Seoul 120-752, Korea; [c]Department of Physiology, College of Medicine, Dongguk University, Gyeongju 780-714, Korea; and [d]Sensory Research Center, Creative Research Initiatives, College of Pharmacy, Seoul National University, Seoul 151-742, Korea

Edited by Richard W. Aldrich, University of Texas, Austin, TX, and approved November 19, 2012 (received for review July 7, 2012)

**Anoctamin 1 (ANO1)/transmembrane protein 16A (TMEM16A) is a calcium-activated anion channel that may play a role in $HCO_3^-$ secretion in epithelial cells. Here, we report that the anion selectivity of ANO1 is dynamically regulated by the $Ca^{2+}$/calmodulin complex. Whole-cell current measurements in HEK 293T cells indicated that ANO1 becomes highly permeable to $HCO_3^-$ at high $[Ca^{2+}]_i$. Interestingly, this result was not observed in excised patches, indicating the involvement of cytosolic factors in this process. Further studies revealed that the direct association between ANO1 and calmodulin at high $[Ca^{2+}]_i$ is responsible for changes in anion permeability. Calmodulin physically interacted with ANO1 in a $[Ca^{2+}]_i$-dependent manner, and addition of recombinant calmodulin to the cytosolic side of excised patches reversibly increased $P_{HCO3}/P_{Cl}$. In addition, the high $[Ca^{2+}]_i$-induced increase in $HCO_3^-$ permeability was reproduced in mouse submandibular gland acinar cells, in which ANO1 plays a critical role in fluid secretion. These results indicate that the $HCO_3^-$ permeability of ANO1 can be dynamically modulated and that ANO1 may play an important role in cellular $HCO_3^-$ transport, especially in transepithelial $HCO_3^-$ secretion.**

Calcium-activated chloride channels (CaCCs) mediate a number of important physiological functions including sensory transduction, regulation of vascular tone, and fluid secretion (1). In the secretory epithelium of airways and exocrine organs, such as intestines, pancreas, and salivary glands, CaCCs control apical efflux of anions, which is essential for the vectorial transport of water and electrolytes in these organs (2, 3). Recently, members of anoctamin (ANO; also known as TMEM16) family, in particular ANO1/TMEM16A and ANO2/TMEM16B, were shown to function as CaCCs in the gut, trachea, salivary glands, and olfactory organs (2–6).

In general, $Cl^-$ channels have nonspecific anion selectivity and permeate other anions in addition to $Cl^-$. In fact, halide ions larger than $Cl^-$, such as $I^-$ and $Br^-$, are more readily permeable to most $Cl^-$ channels. For example, the anion selectivity sequence of both endogenous CaCCs and heterologously expressed ANO1 is $I^- > Br^- > Cl^- > HCO_3^- > F^-$ (3, 7). However, in physiological conditions, the two most abundant anions that can be the charge carrier of anion channels are $Cl^-$ and $HCO_3^-$. Although the permeation and conduction mechanisms of $Cl^-$ via anion channels are fairly well characterized, those of $HCO_3^-$ are poorly understood. It has been demonstrated that a significant proportion of transepithelial $HCO_3^-$ transport is mediated by electrodiffusive pathways, suggesting that anion channels are involved in this process (8–10). Up to this point, neither molecular nor physiological experiments have demonstrated the presence of bona fide selective $HCO_3^-$ channels. Therefore, it is generally believed that nonspecific anion channels mediate electrodiffusive $HCO_3^-$ transport.

$HCO_3^-$, as a major component of the $CO_2/HCO_3^-$ buffer system, is an indispensible ingredient in our body fluids that guards against toxic intracellular and extracellular fluctuations in pH (11). In addition, as a chaotropic ion, $HCO_3^-$ facilitates the solubilization of macromolecules in biological fluids and stimulates mucin secretion (11, 12). Indeed, recent progress in epithelial pathophysiology has indicated that aberrant $HCO_3^-$ secretion is associated with a spectrum of diseases in the respiratory, gastrointestinal, and genitourinary systems, such as cystic fibrosis, pancreatitis, and infertility (10, 11, 13, 14). In the present study, we provide evidence that $Ca^{2+}$/calmodulin dynamically regulates the anion selectivity and $HCO_3^-$ permeability of ANO1 by using integrated molecular and physiological approaches. These results offer insight into how transepithelial $HCO_3^-$ transport is activated, in particular in response to cytosolic $Ca^{2+}$ signaling, and offer a therapeutic strategy for the treatment of diseases derived from aberrant $HCO_3^-$ secretion.

## Results

**$HCO_3^-$ Permeability of ANO1.** CaCCs in native epithelial cells exhibit distinct features according to intracellular $Ca^{2+}$ levels. At submaximal cytosolic $Ca^{2+}$ levels of ~1 μM $[Ca^{2+}]_i$, CaCCs elicit strong outward rectifications and time-dependent activation, whereas at higher $[Ca^{2+}]_i$, the current-voltage (I-V) relationship becomes linear and the time dependency disappears (15, 16). As shown in Fig. S1, whole-cell current measurements of hANO1 overexpressed in HEK 293T cells that had been stimulated with 400 nM and 3 μM free $Ca^{2+}$-containing pipette solutions reproduced these characteristic features of CaCCs (17). The following three findings verified that the currents obtained in HEK 293T cells were mostly from transfected ANO1: (*i*) the currents were inhibited by the ANO1/TMEM16A-inhibitor $T16A_{inh}$-A01 (18) (Fig. S1 *A* and *B*); (*ii*) the currents obtained in the control cells transfected with mock vectors were negligible (Fig. S1 *A* and *B*); and (*iii*) the permeabilities of ANO1 to cations were minimal compared with that to chloride (Fig. S1*C*).

We next assessed the permeability of ANO1 to $HCO_3^-$ by replacing 150 mM extracellular $Cl^-$ with 130 mM $HCO_3^-$ and 20 mM $Cl^-$ in whole-cell current measurements (Fig. 1). The $HCO_3^-/Cl^-$ permeability ratio ($P_{HCO3}/P_{Cl}$) was determined from the shift of reversal potential ($\Delta E_{rev}$) by using the Goldman–Hodgkin–Katz equation (7, 19, 20). Because ANO1 has two distinct kinetics depending on $[Ca^{2+}]_i$, $HCO_3^-$ permeabilities at both submaximal (400 nM) and higher (3 μM) $[Ca^{2+}]_i$ were analyzed. In current measurements with a 400 nM free $Ca^{2+}$-containing pipette, replacing the bath side with a 130 mM $HCO_3^-$-containing solution induced a 21.4 ± 1.1 mV positive shift in $\Delta E_{rev}$, indicating that ANO1 was more readily permeable to $Cl^-$ than to $HCO_3^-$ and that $P_{HCO3}/P_{Cl}$ was only 0.35 ± 0.02 (Fig. 1*A*). The protocol was repeated with pipettes containing 3 μM free $Ca^{2+}$. Surprisingly, at 3 μM free $Ca^{2+}$, replacing the bath solution with 130 mM $HCO_3^-$ induced a negligible change in $E_{rev}$ ($\Delta E_{rev} = -0.9 \pm 0.5$ mV), indicating that the $HCO_3^-$ permeability of ANO1 was greatly increased and was comparable to that of $Cl^-$ ($P_{HCO3}/P_{Cl} = 1.04 \pm 0.02$) (Fig. 1*B*). The $EC_{50}$ value of $[Ca^{2+}]_i$ for $P_{HCO3}/P_{Cl}$ increase was

Author contributions: M.G.L. designed research; J.J., J.H.N., and H.W.P. performed research; U.O. and J.-H.Y. contributed new reagents/analytic tools; J.J. and M.G.L. analyzed data; and J.J. and M.G.L. wrote the paper.

The authors declare no conflict of interest.

This article is a PNAS Direct Submission.

[1]To whom correspondence should be addressed. E-mail: mlee@yuhs.ac.

This article contains supporting information online at www.pnas.org/lookup/suppl/doi:10.1073/pnas.1211594110/-/DCSupplemental.

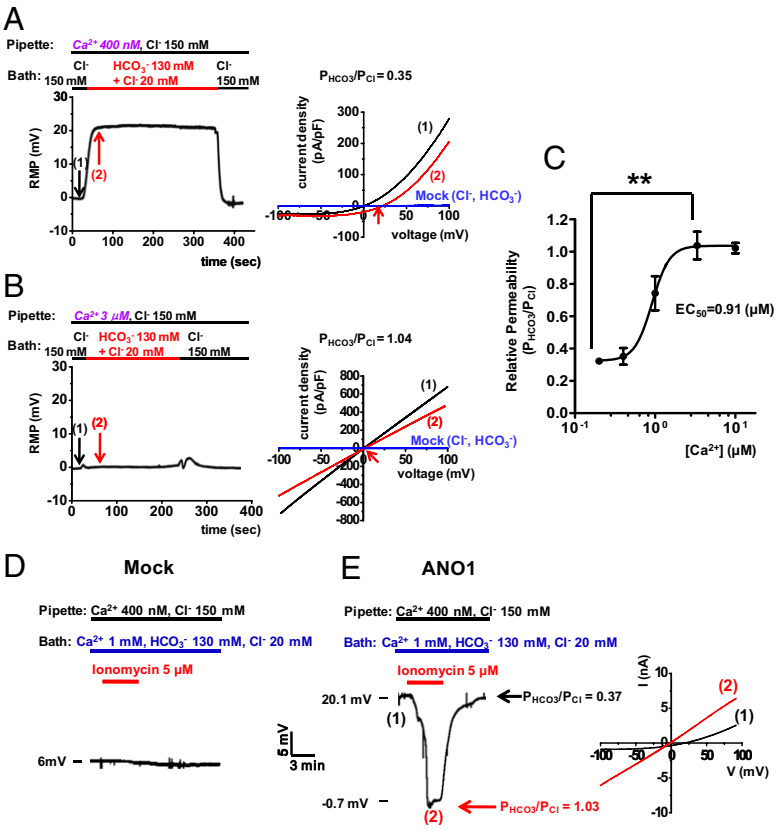


**Fig. 1.** High $[Ca^{2+}]_i$ increases the $HCO_3^-$ permeability of ANO1. Whole-cell currents were measured in HEK 293T cells transfected with pCMV-hANO1. (*A*) Representative traces of resting membrane potential (RMP) measurements with a 400 nM free $Ca^{2+}$-containing pipette (*Left*) and the I-V relationship at the indicated points (*Right*) are shown. Replacing the bath side with a high $HCO_3^-$-containing solution (130 mM) induced a 21.4 ± 1.1 mV ($n$ = 10) positive shift in $\Delta E_{rev}$, indicating that $P_{HCO3}/P_{Cl}$ was only 0.35 ± 0.02. (*B*) When measured with a 3 μM free $Ca^{2+}$-containing pipette, replacing the bath with a 130 mM $HCO_3^-$ solution induced a negligible change in $E_{rev}$ ($\Delta E_{rev}$ = −0.9 ± 0.5 mV, $n$ = 14), indicating that the $HCO_3^-$ permeability of ANO1 was comparable to that of $Cl^-$ ($P_{HCO3}/P_{Cl}$ = 1.04 ± 0.02). Endogenous $Cl^-$ and $HCO_3^-$ currents (Mock), that were negligible at both low and high $[Ca^{2+}]_i$, did not affect the reversal potential. (*C*) The dose–response relationship of $[Ca^{2+}]_i$ and $P_{HCO3}/P_{Cl}$ ($n$ = 5–14 at each point). (*D* and *E*) $[Ca^{2+}]_i$-induced changes in $P_{HCO3}/P_{Cl}$ were dynamically monitored by using the $Ca^{2+}$ ionophore ionomycin. Control cells transfected with mock vectors did not exhibit any changes in RMP during ionomycin treatment (*D*). When $[Ca^{2+}]_i$ was initially clamped at 400 nM in ANO1-expressing cells, RMP equaled 20.1 ± 0.1 mV ($P_{HCO3}/P_{Cl}$ = 0.37 ± 0.01, $n$ = 5). Treatment with ionomycin (5 μM), which increases $Ca^{2+}$ signaling, decreased RMP to −0.7 ± 0.3 mV ($P_{HCO3}/P_{Cl}$ = 1.03 ± 0.01). Removing ionomycin reversed RMP to 20.0 ± 0.3 mV (*E*).

0.91 μM in the $Ca^{2+}$-ethylene glycol tetraacetic acid (EGTA) solutions (Fig. 1*C*). The $Ca^{2+}$-buffering capacity of EGTA may be weakened at >1 μM free $Ca^{2+}$ or affected by pH. However, the $EC_{50}$ value in the $Ca^{2+}$-EGTA solutions was not different from those buffered with multiple combinations of the high-affinity and low-affinity $Ca^{2+}$ chelators (Fig. S2 *A* and *B*). Furthermore, direct measurments of $Ca^{2+}$ concentrations using fluorescent probes confirmed that the free $Ca^{2+}$ concentrations of $Ca^{2+}$-EGTA buffers were within acceptable ranges of up to 10 μM (Fig. S2*C*). In addition, the basic properties of the ANO1 $Cl^-$ channel measured with the pH-insenstive $Ca^{2+}$ buffers BAPTA (for 400 nM $[Ca^{2+}]_i$) and dibromo-BAPTA (for 3 μM $[Ca^{2+}]_i$) were comparable to those measured with the EGTA buffers (Fig. S2 *D* and *E*). Therefore, to avoid possible confounding variables derived from the use of different chelators at each $Ca^{2+}$ concentration, we continued to use the $Ca^{2+}$-EGTA buffer for further experiments.

Experiments with the $Ca^{2+}$ ionophore ionomycin revealed the dynamic change of $P_{HCO3}/P_{Cl}$ induced by $[Ca^{2+}]_i$ (Fig. 1 *D* and *E*). In these experiments, the pipette solution contained 150 mM $Cl^-$, and the bath contained 130 mM $HCO_3^-$, 20 mM $Cl^-$, and 1 mM $Ca^{2+}$. When ANO1 was stimulated with a submaximal-free $Ca^{2+}$ concentration of 400 nM in the pipette, the resting membrane potential (RMP) was 20.1 ± 0.1 mV, resulting in a $P_{HCO3}/P_{Cl}$ value of 0.37 ± 0.01 (Fig. 1*E*). The addition of ionomycin (5 μM), which induces higher $Ca^{2+}$ signaling as confirmed by the linear I-V relationship (Fig. 1*E, Right*), decreased RMP to −0.7 ± 0.3 mV, indicating that $P_{HCO3}/P_{Cl}$ increased to 1.03 ± 0.01. Notably, removing ionomycin dynamically reversed RMP to 20.0 ± 0.3 mV.

**$[Ca^{2+}]_i$ and a Cytosolic Factor Increase the Dielectric Constant of the ANO1 Selectivity Filter.** ANO1 and native CaCCs have been shown to permeate various anions (3, 7). Therefore, we examined whether an increase in $[Ca^{2+}]_i$ also affects the permeability of other anions. Initially, the protocols used in Fig. 1*E* were repeated to measure $I^-$ permeability. In contrast to $HCO_3^-$, a bath solution rich in $I^-$ evoked a negative RMP of −27.4 ± 0.3 mV at 400 nM free $Ca^{2+}$, suggesting that $I^-$ influx is larger than $Cl^-$ efflux ($P_I/P_{Cl}$ = 2.71 ± 0.03). Notably, ionomycin treatment increased RMP to −9.8 ± 1.4 mV, hence decreasing $P_I/P_{Cl}$ to 1.54 ± 0.07 (Fig. 2*B*). We further analyzed the changes in selectivity for other anions by using the protocols used in Fig. 1 *A* and *B*. Representative traces are shown in Fig. S3, and summarized results are presented in Fig. 2*C*. At 400 nM free $Ca^{2+}$, the permeability sequence of anions was $I^- > NO_3^- > Br^- > Cl^- > HCO_3^- > F^-$. This permeability order was not altered at 3 μM free $Ca^{2+}$, except that $HCO_3^-$ permeability was equal to or slightly greater than that of $Cl^-$. However, the intervals of the relative permeabilities between anions became smaller and the value of $P_X/P_{Cl}$ converged to 1 when $[Ca^{2+}]_i$ was increased in whole-cell patch clamp recordings. Interestingly, this finding was not observed in excised patches. In outside-out (Fig. 2*D* and Fig. S4) or inside-out (Fig. S5) patches, $P_X/P_{Cl}$ values at 3 μM or even 10 μM free $Ca^{2+}$ were almost identical to those at 400 nM free $Ca^{2+}$. These results indicate that a cytosolic factor is involved in the $[Ca^{2+}]_i$-induced alterations in ANO1 anion permeability.

To explore the mechanisms of permeability changes, we calculated the dielectric constant of the hypothetical anion selectivity filter of ANO1. Many anion channels, including CaCCs and the cystic fibrosis transmembrane conductance regulator (CFTR), exhibit a so-called "lyotropic" or Hofmeister series of ion selectivity. It has been suggested that the pore of these channels has a large polarizable tunnel, where ion selectivity is basically determined by the hydration energy of ions (7, 20). Therefore, the channel is more permeable to large anions that are more readily dehydrated. In this case, an important parameter that governs the interaction between anions and the channel filter is the dielectric constant (relative permittivity, ε) (20, 21). Interestingly, ε of ANO1 increased from 13 to 18 when $[Ca^{2+}]_i$ was increased in whole-cell recordings (Fig. S3*G*). However, in outside-out patches, ε was constant (ε = 12) regardless of changes in $[Ca^{2+}]_i$ (Fig. S4*G*). Taken together, these findings imply that

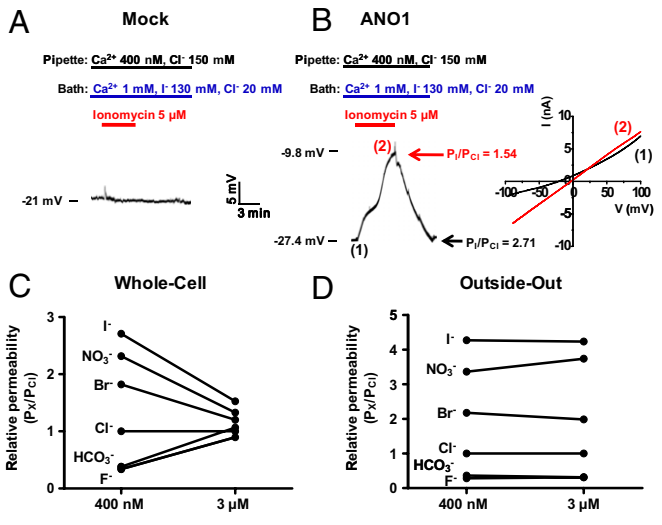


**Fig. 2.** $[Ca^{2+}]_i$ and a cytosolic factor modulate the anion selectivity of ANO1. (*A* and *B*) $P_I/P_{Cl}$ was monitored by using the protocols shown in Fig. 1 *D* and *E*. Control cells transfected with mock vectors did not exhibit any changes in RMP during ionomycin treatment (*A*). In ANO1-expressing cells, a bath solution rich in $I^-$ evoked a negative RMP of −27.4 ± 0.3 mV ($P_I/P_{Cl}$ = 2.71 ± 0.03, $n$ = 4) at a free $Ca^{2+}$ concentration of 400 nM. Treatment with ionomycin increased RMP to −9.8 ± 1.4 mV ($P_I/P_{Cl}$ = 1.54 ± 0.07), indicating that $I^-$ permeability is also altered by high $[Ca^{2+}]_i$. (*C* and *D*) The anion selectivity of ANO1 was examined by using the protocols shown in Fig. 1 *A* and *B*. ($n$ = 5–6 per substitute anion). Representative traces of whole-cell and outside-out patch recordings are presented in Figs. S3 and S4, respectively. Note that intervals of the relative permeabilities between anions became smaller and that the value of $P_X/P_{Cl}$ converged to 1 when $[Ca^{2+}]_i$ was increased in the whole-cell recordings (*C*), but not in outside-out patch recordings (*D*).

a cytosolic factor increases the polarizability of ANO1 selectivity filter in response to $[Ca^{2+}]_i$, which then alters the anion permeation pattern of ANO1.

**Calmodulin Modulates ANO1 $HCO_3^-$ Permeability via a Direct Physical Interaction.** Next, we investigated the identity of cytosolic factor that alters the anion permeability of ANO1. Recently, it has been shown that with no K (lysine) protein kinase-1 (WNK1)/Ste20-related proline/alanine-rich kinase (SPAK) regulate the $HCO_3^-$ permeability of CFTR (19). However, this mechanism did not hold true for ANO1. WNK1/SPAK overexpression did not affect $P_{HCO3}/P_{Cl}$ of ANO1 (Fig. S6 *A* and *B*). Phosphorylation, which adds negative charges to proteins, can potentially alter ε of the anion filter. However, ATP depletion in whole-cell current measurements, which can inhibit protein phosphorylation, did not affect $P_{HCO3}/P_{Cl}$. Furthermore, treatment with K252a (broad-spectrum serine/threonine kinase inhibitor), KN-93 (CAMKII inhibitor), and genistein (nonspecific tyrosine kinase inhibitor) did not significantly change $P_{HCO3}/P_{Cl}$ (Fig. S6*C*). In addition, phosphatidylinositol 4,5-bisphosphate ($PIP_2$), which has been demonstrated to regulate the activity of many ion channels (22), did not affect $P_{HCO3}/P_{Cl}$ (Fig. S6*D*).

Calmodulin functions as a calcium sensor for many cellular events ranging from cell cycle regulation to ion channel activation (23, 24). Interestingly, treatment with J-8, which inhibits the binding between calmodulin and target proteins, reversibly inhibited the high $[Ca^{2+}]_i$-induced increase in $P_{HCO3}/P_{Cl}$ (Fig. S6 *E* and *F*). To further identify the involvement of calmodulin in ANO1 $HCO_3^-$ permeability, whole-cell currents were measured in cells treated with siRNAs against calmodulin. In humans, three separate genes with 100% amino acid identity encode calmodulins (24). As shown in Fig. 3 *A*–*D*, silencing of calmodulin by treatment with siRNAs against all three calmodulin genes decreased $P_{HCO3}/P_{Cl}$ at 3 μM free $Ca^{2+}$ from 1.01 ± 0.05 to 0.59 ± 0.05, indicating that calmodulin is required for the high $[Ca^{2+}]_i$-induced increase in $P_{HCO3}/P_{Cl}$ of ANO1. In addition, GST pull-down assays with diverse free $Ca^{2+}$ concentrations revealed that ANO1 physically interacts with calmodulin in a $Ca^{2+}$-dependent manner, being prominent at >1 μM free $Ca^{2+}$ (Fig. 3 *E* and *F*). Furthermore, the addition of recombinant calmodulin to the cytosolic side of outside-out patches sufficiently increased $P_{HCO3}/P_{Cl}$ at 3 μM free $Ca^{2+}$ from 0.39 ± 0.04 to 0.97 ± 0.06 (Fig. 4 *A*–*C*). This result was more dynamically seen in the inside-out patches. Addition and removal of recombinant calmodulin to the bath (cytosolic side of inside-out patch) reversibly increased $P_{HCO3}/P_{Cl}$ (Fig. 4 *D* and *E*) and reduced $P_I/P_{Cl}$ (Fig. S7). Taken together, these findings indicate that calmodulin modulates $P_{HCO3}/P_{Cl}$ in response to $[Ca^{2+}]_i$ via a direct physical interaction with ANO1.

**Calmodulin Binding Motifs of ANO1.** Next, we determined the motif(s) of ANO1 responsible for its interaction with calmodulin. Two putative calmodulin-binding motifs (CBM1-2), both of which belong to the $Ca^{2+}$-dependent "1-8-14 motif" family (24) and display high conservation among vertebrates, were identified by a prediction program (http://calcium.uhnres.utoronto.ca/ctdb/ctdb/home.html) (Fig. 5 *A* and *B*). Pull-down assays using the I317A and I762A mutants of ANO1, in which critical hydrophobic residues at position 1 or 14 of CBMs were abolished, revealed a weakened association between the ANO1 mutants and calmodulin (Fig. 5*C*). Furthermore, the I317A and I762A mutations reduced $P_{HCO3}/P_{Cl}$ with a partial additive effect in whole-cell measurements at 3 μM free $Ca^{2+}$ (Fig. 5*D* and Fig. S8 *A*–*D*), indicating that these motifs are involved in the calmodulin

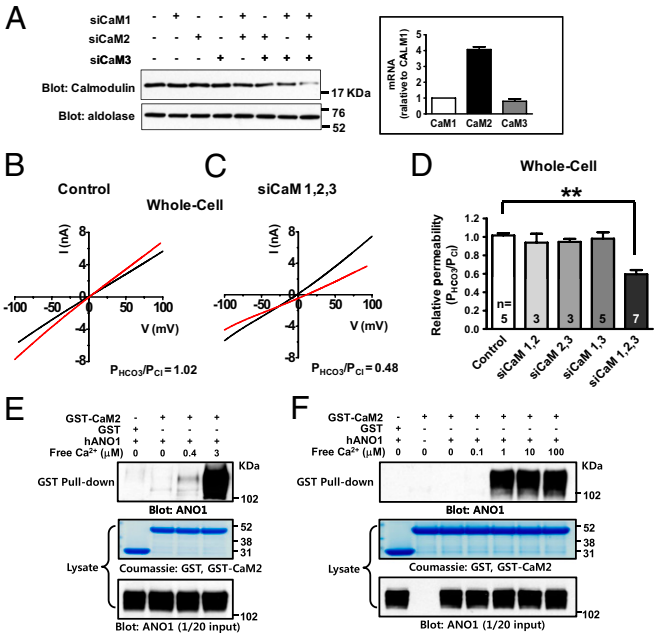


**Fig. 3.** Calmodulin is required for the high $[Ca^{2+}]_i$-induced increase in $P_{HCO3}/P_{Cl}$ of ANO1. (*A*) The expression of the endogenous calmodulin (CaM) 1, 2, and/or 3 gene(s) was inhibited by treatment with gene-specific siRNAs. Silencing of all three CaM genes reduced the protein expression of calmodulin by 87 ± 5%. (*A Inset*) results of quantitative RT-PCR assays illustrate that CaM2 is the major isoform expressed in HEK 293T cells. (*B*–*D*) Whole-cell recordings were performed with a 3 μM free $Ca^{2+}$-containing pipette. Silencing of all three CaM genes reduced the high $[Ca^{2+}]_i$-induced increase in $P_{HCO3}/P_{Cl}$ of ANO1 (Control: 1.01 ± 0.05; siCaM 1,2,3: 0.59 ± 0.05). $^{**}P < 0.01$. (*E* and *F*) GST pull-down assays were performed with recombinant GST-calmodulin2 (CaM2) protein and cell lysates prepared from HEK 293T cells expressing ANO1. The free $Ca^{2+}$ concentrations in the binding buffer were tightly controlled by using EGTA and $CaCl_2$. ANO1 associates with calmodulin in a $Ca^{2+}$-dependent manner, in particular at free $Ca^{2+}$ concentrations >1 μM.

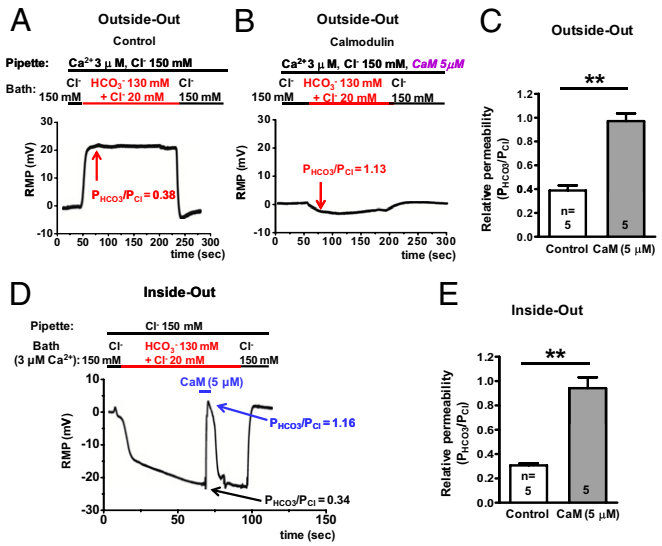


**Fig. 4.** Supplementation of recombinant calmodulin in excised patches sufficiently reproduced the high $[Ca^{2+}]_i$-induced increase in $P_{HCO3}/P_{Cl}$ of ANO1. (*A–C*) In outside-out excised patches, the addition of purified calmodulin protein (CaM) in a 3 μM free $Ca^{2+}$-containing pipette solution increased $P_{HCO3}/P_{Cl}$ from 0.39 ± 0.09 to 0.97 ± 0.06. (*D* and *E*) In inside-out excised patches, the addition and removal of CaM in a 3 μM free $Ca^{2+}$-containing bath solution (cytosolic side) reversibly increased $P^{HCO3}/P_{Cl}$ from 0.31 ± 0.02 to 0.94 ± 0.09. $^{**}P < 0.01$.

binding and regulation of ANO1 $HCO_3^-$ permeability. However, the I317A+I762A ANO1 mutant exhibited no significant difference from the wild-type ANO1 in the $[Ca^{2+}]_i$ sensitivity of ANO1 $Cl^-$ currents, indicating that the I317A+I762A mutation did not affect the $Ca^{2+}$-induced activation process of ANO1 (Fig. S8*E*).

Lastly, pull-down assays and outside-out patch experiments were performed with short peptides corresponding to the sequences of CBM1 and CBM2. In pull-down assays, treatment with CBM1 or CBM2 peptide profoundly weakened the association between ANO1 and calmodulin via quenching the cytosolic pool of calmodulin (Fig. 5*E*), indicating that CBM1 and CBM2 separately have calmodulin-binding activity. The independent calmodulin-binding activity of CBM1 and CBM2 was also confirmed with another $Ca^{2+}$/calmodulin binding client mGluR5 (Fig. S9). Notably, depletion of free cytosolic calmodulin by CBM1 or CBM2 peptide inhibited the $Ca^{2+}$/calmodulin-induced up-regulation of $P_{HCO3}/P_{Cl}$ (Fig. 5*F* and Fig. S10).

**CaCC and $HCO_3^-$ Permeability in Mouse Salivary Gland Acinar Cells.** ANO1 was demonstrated to mediate CaCC activity in mouse salivary gland acinar cells (2, 3). Therefore, the high $[Ca^{2+}]_i$-induced regulation of ANO1 permeability to $HCO_3^-$ was examined in mouse submandibular gland (SMG) acinar cells as a model in vivo system. SMG acinar cells were harvested as detailed in *SI Materials and Methods*. Immunoblotting with an anti-ANO1 antibody revealed that ANO1 is abundantly expressed in the SMG (Fig. 6*A*). Whole-cell currents measured in single SMG acinar cells exhibited typical CaCC patterns at 400 nM and 3 μM free $Ca^{2+}$, and these currents were fully inhibited by the ANO1 inhibitor T16Ainh-A01 (Fig. 6 *B* and *C*). Importantly, increment in the free $Ca^{2+}$ concentration in the pipette from 400 nM to 3 μM increased $P_{HCO3}/P_{Cl}$ from 0.43 ± 0.10 to 0.89 ± 0.09 (Fig. 6 *D–F*), similar to the findings observed in HEK 293T cells expressing ANO1. In addition, RMP measurements also revealed that ionomycin treatment dynamically increased $P_{HCO3}/P_{Cl}$ from 0.38 to 0.97 (Fig. 6*G*). Therefore, high $[Ca^{2+}]_i$ up-regulates the $HCO_3^-$ permeability of CaCCs in secretory epithelial cells.

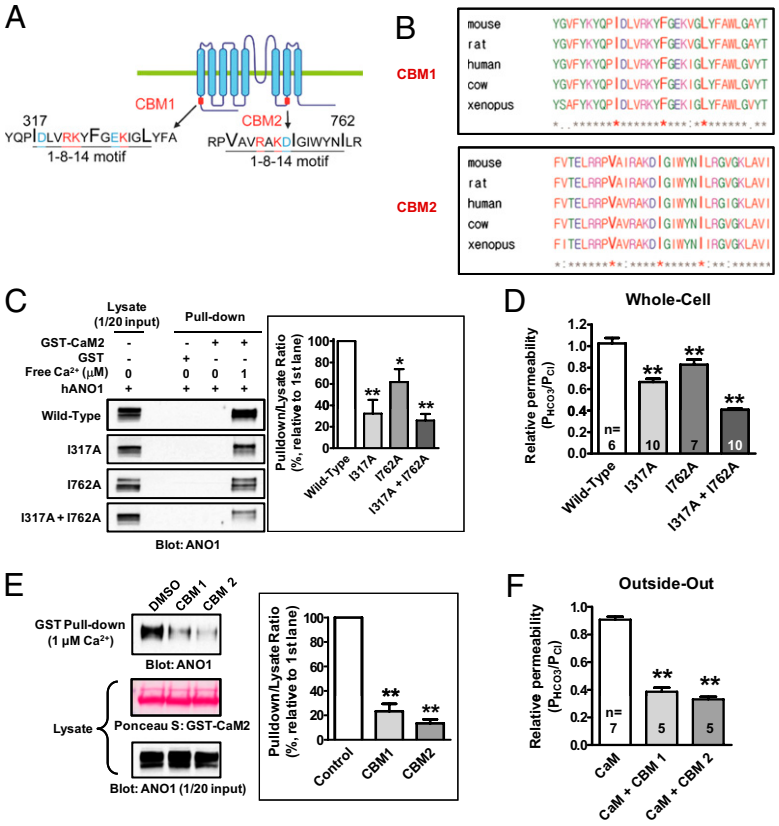


**Fig. 5.** Calmodulin-binding motifs (CBMs) of ANO1. (*A* and *B*) Two putative calmodulin-binding motifs (CBM1 and CBM2) of hANO1/TMEM16A (*ac* isoform) that belong to the $Ca^{2+}$-dependent 1-8-14 motif were identified by a computational search. These motifs were highly conserved among vertebrate ANO1 proteins (*B*). (*C*) GST pull-down assays were performed with recombinant GST-calmodulin2 (CaM2) protein and cell lysates prepared from HEK 293T cells expressing the wild-type and mutant ANO1s. ANO1-calmodulin binding intensities at 1 μM free $Ca^{2+}$ were decreased by the I371A and/or I762A mutations, in which critical hydrophobic residues at position 1 or 14 of the CBMs were abolished. (*D*) Effects of the I317A and/or I762A mutation(s) on $P_{HCO3}/P_{Cl}$ of ANO1 were analyzed in the whole-cell configuration by using a 3 μM free $Ca^{2+}$-containing pipette. Measurement conditions and representative traces are shown in Fig. S8 *A–D*. The I317A mutation in CBM1 and I762A mutation in CBM2 additively reduced $P_{HCO3}/P_{Cl}$. (*E*) GST pull-down assays were performed with short peptides corresponding to the sequences of CBM1 and CBM2. CBM1 or CBM2 peptide independently weakened the association between ANO1 and calmodulin at 1 μM free $Ca^{2+}$. (*F*) The effects of CBM peptides on the $Ca^{2+}$/calmodulin-induced up-regulation of ANO1 $P_{HCO3}/P_{Cl}$ were analyzed in outside-out patches by using a 3 μM free $Ca^{2+}$-containing pipette. Detailed measurement conditions and representative traces are shown in Fig. S10. CBM1 or CBM2 peptide independently inhibited the calmodulin-induced up-regulation of $P_{HCO3}/P_{Cl}$. $^{*}P < 0.05$, $^{**}P < 0.01$.

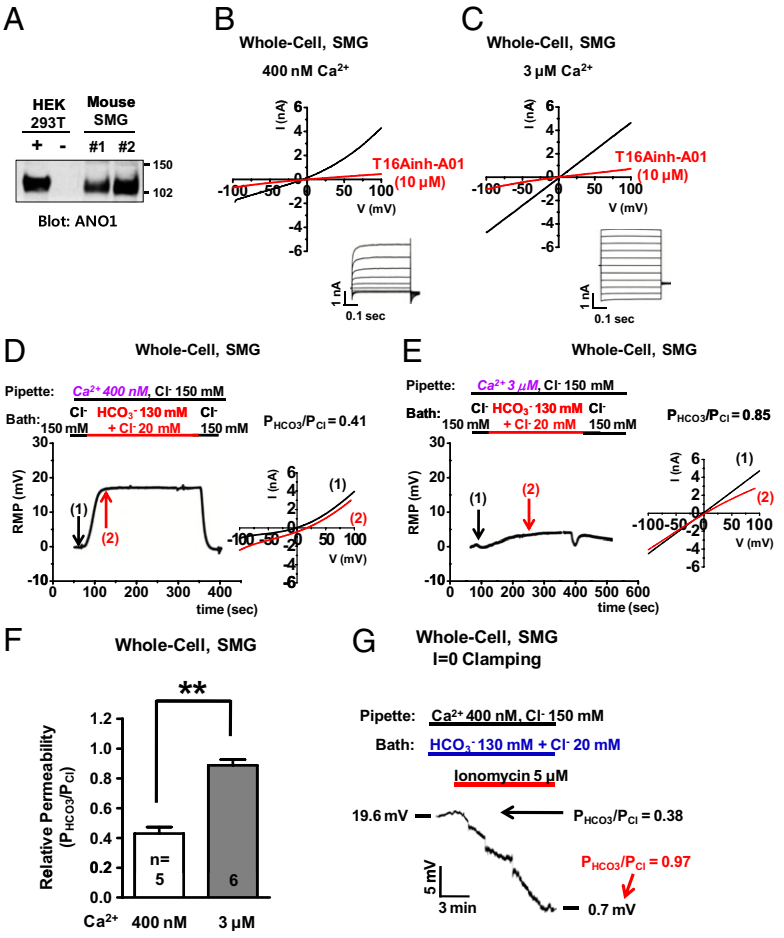


**Fig. 6.** High $[Ca^{2+}]_i$ increases the $HCO_3^-$ permeability of CaCCs in mouse submandibular gland (SMG) acinar cells. (*A*) SMG acinar cells were freshly isolated and immunoblotted by using anti-ANO1/TMEM16A antibody. Protein samples from HEK 293T cells transfected with pCMV-hANO1 and mock plasmids were used as positive and negative controls, respectively. (*B* and *C*) Whole-cell current recordings of CaCCs in SMG acinar cells were performed with pipettes containing 400 nM or 3 μM free $Ca^{2+}$. I-V curves were obtained by applying ramp pulses (0.2 mV/ms) or step pulses (voltage interval; 20 mV, duration; 0.5 s) from −100 to +100 mV. At 400 nM $[Ca^{2+}]_i$, an outwardly rectifying and time-dependent $Cl^-$ current was generated, and this current was inhibited by $T16A_{inh}$-A01 (10 μM). When $[Ca^{2+}]_i$ was increased to 3 μM, the current became linear and time-independent. (*D–F*) $P_{HCO3}/P_{Cl}$ of CaCC in SMG acinar cells was examined by using protocols shown in Fig. 1 *A* and *B*. An increment in the pipette free $Ca^{2+}$ from 400 nM to 3 μM increased $P_{HCO3}/P_{Cl}$. A summary of multiple experiments with indicated numbers are presented in *F*. (*G*) $P_{HCO3}/P_{Cl}$ was dynamically monitored in SMG acinar cells by using the protocols shown in Fig. 1*E*. Treatment with ionomycin (5 μM) decreased RMP from 19.6 to 0.7 mV, indicating that $P_{HCO3}/P_{Cl}$ was increased from 0.38 to 0.97.

## Discussion

In this study, we provide molecular and physiological evidence that ANO1 anion selectivity is dynamically modulated by $Ca^{2+}$/calmodulin. When measured in whole-cell configurations, $P_{HCO3}/P_{Cl}$ and the dielectric constant of hypothetical anion selectivity filter increased in response to elevated $[Ca^{2+}]_i$ (Fig. 2 and Figs. S3 and S4). Given that changes in the $P_{HCO3}/P_{Cl}$ and anion selectivity were not observed in excised patches, we hypothesized that electrostatic alterations in the selectivity filter are not directly induced by $Ca^{2+}$; instead, these alterations may require a cytosolic factor. Further experiments revealed that calmodulin is both necessary and sufficient to induce changes in the anion selectivity of ANO1 (Figs. 3–6).

Calmodulin participates in diverse critical cellular functions such as cytoskeletal organization, cell division, and regulation of membrane receptors and transporters (23, 24). These effects of calmodulin can be mediated by either $Ca^{2+}$-dependent or -independent interactions with target proteins. Increases in $[Ca^{2+}]_i$ promote interactions between calmodulin and target proteins that have $Ca^{2+}$-dependent CBMs (24). ANO1 possesses two 1-8-14-type $Ca^{2+}$-dependent CBMs that contain conserved hydrophobic residues and positively charged amino acids within the motif. Consequently, pull-down assays revealed a direct interaction between calmodulin and ANO1 at high free $Ca^{2+}$ concentrations (Fig. 3). The dissociation constant ($K_d$) of $Ca^{2+}$-calmodulin binding is estimated to be ~1 μM (25, 26), which is similar to the $EC_{50}$ of $P_{HCO3}/P_{Cl}$ modulation (Fig. 1*C*) and affinities of ANO1-calmodulin association (Fig. 3 *E* and *F*) in the present study, indicating that ANO1 associates with the $Ca^{2+}$-bound form of calmodulin. Therefore, at $[Ca^{2+}]_i > 1$ μM, $Ca^{2+}$/calmodulin binds to ANO1 and affects the polarizability of its anion filter. This alteration in polarizability eventually causes changes in the permeation pattern of ANO1 observed in the present study (Fig. 2).

Interestingly, it has been suggested that ANO channels may have multiple anion selectivity. For example, *Xenopus* ANO1 has been shown to have multiple open states that differ in kinetics and anion selectivity (5). It will be interesting to see whether the $Ca^{2+}$/calmodulin-induced change of anion permeability shown in the present study is associated with different open states of ANO1. In a previous study, ANO2/TMEM16b in mouse olfactory neurons showed a time-dependent change in anion selectivity during intracellular calcium signaling evoked by photorelease of caged $Ca^{2+}$, although its physiological significance was not fully understood (30). Because mammalian ANO2s have a high homology with ANO1 and retain the two CBMs, it is expected that $HCO_3^-$ permeability of ANO2 would also be dynamically regulated by $Ca^{2+}$/calmodulin.

An intriguing finding to add is that calmodulin is not associated with the rectification behavior of ANO1. In excised patches, although a high free $Ca^{2+}$ concentration did not affect $P_X/P_{Cl}$, it clearly induced a linear I-V relationship of ANO1 currents similar to that observed in whole-cell measurements (Figs. S4 and S5). This result suggests that increases in $[Ca^{2+}]_i$ itself, but not calmodulin, are responsible for the high $[Ca^{2+}]_i$-induced change in the rectification pattern of ANO1. In fact, it has been assumed that a calcium-binding site is located within the membrane electric field of CaCCs and facilitating calcium binding to the channel at a positive voltage is attributable to the linear I-V relationship at high $[Ca^{2+}]_i$ (1, 5, 27).

ANO1 has several splice variants. Protein segments that are alternatively expressed are termed *a* (116 residues), *b* (22 residues), *c* (4 residues), and *d* (26 residues) (28). Tian et al. (29) suggested that calmodulin increases the activity of ANO1/

TMEM16A in an experiment by using ANO1 with *abc* segments. In their study, a calmodulin-binding site that does not belong to the 1-8-14 type is mapped to a region that overlaps segment *b* and this region is responsible for the calmodulin-induced increase in current amplitude. However, the ANO1 protein used in the present study only has segments *a* and *c* and does not contain segment *b*, and its $Ca^{2+}$ sensitivity is not affected by ablation of calmodulin-binding sites (Fig. S8*E*). Interestingly, segment *b* is absent in the ANO1 expressed in many tissues where $HCO_3^-$ secretion plays an important role, such as the lungs, colon, and salivary glands (3, 28). These results imply that calmodulin-induced modulation of anion selectivity has a more central role in the regulation of ANO1, especially in $HCO_3^-$-secreting epithelia.

Epithelial cells in respiratory, gastrointestinal, and genitourinary systems secrete $HCO_3^-$-containing fluids, which include saliva, pancreatic juice, intestinal fluids, airway surface fluid, and fluids secreted by reproductive organs (11). $HCO_3^-$ is an essential ingredient in these fluids and plays critical roles. For example, in cystic fibrosis, aberrant $HCO_3^-$ secretion leads to altered mucin hydration and solubilization, resulting in a thick mucus that frequently blocks ductal structures of the internal organs (31). However, the precise mechanisms explaining how anion channels mediate epithelial $HCO_3^-$ secretion in response to physiological stimuli remain elusive in most circumstances.

We demonstrated that a dynamic increase in the ANO1 $HCO_3^-$ permeability was induced by cytosolic calcium signals in SMG acinar cells and in model cells (Fig. 6). Cholinergic stimulation, which evokes an increase in $[Ca^{2+}]_i$, is known to induce $HCO_3^-$ secretion via $Cl^-$ channels in rat and human salivary gland cells (32, 33). Furthermore, salivary $HCO_3^-$ secretion in humans is greatly increased during chewing, which induces vagal cholinergic activation (34). In the apical microdomain of secretory epithelial cells where $IP_3$ receptors and CaCCs are clustered (2, 35), $[Ca^{2+}]_i$ is estimated to be increased by physiological stimuli to levels as high as 50 μM (36, 37). These results, taken together, suggest that an increase in ANO1 $P_{HCO3}/P_{Cl}$ would be a major mechanism of epithelial $HCO_3^-$ secretion in response to cytosolic calcium signals. It is important to mention that CaCCs are also expressed in the apical membrane of respiratory and pancreatic epithelia (3), in which defective CFTR-mediated $HCO_3^-$ secretion causes cystic fibrosis and chronic pancreatitis (13, 19). Further identification of the critical mechanisms and components involved in ANO1-mediated $HCO_3^-$ secretion is expected to provide a pharmacologically suitable target for treating diseases caused by aberrant $HCO_3^-$ secretion.

## Materials and Methods

Procedures and materials for cell culture, isolation of mouse SMG cells, electrophysiology, quantitative PCR, and pull-down assay are fully described in *SI Materials and Methods*. The results of multiple experiments are presented as means ± SEM. Statistical analysis was performed by using Student's *t* tests or analysis of variance followed by Tukey's multiple comparison test as appropriate. $P < 0.05$ was considered statistically significant.

**ACKNOWLEDGMENTS.** We thank Drs. A. S. Verkman and C. H. Kim for kindly providing $T16A_{inh}$-A01 and pcDNA3.1-rCalmodulin2. This work was supported by the National Research Foundation, the Ministry of Education, Science, and Technology (Korea) Grants 2011-0001178 and 2011-0016484 and National Project for Personalized Genomic Medicine, Korea Health 21 R&D Project, Ministry of Health & Welfare (Korea) Grant A111218-11-PG03.

1. Hartzell C, Putzier I, Arreola J (2005) Calcium-activated chloride channels. *Annu Rev Physiol* 67:719–758.
2. Romanenko VG, et al. (2010) Tmem16A encodes the $Ca^{2+}$-activated $Cl^-$ channel in mouse submandibular salivary gland acinar cells. *J Biol Chem* 285(17):12990–13001.
3. Yang YD, et al. (2008) TMEM16A confers receptor-activated calcium-dependent chloride conductance. *Nature* 455(7217):1210–1215.
4. Caputo A, et al. (2008) TMEM16A, a membrane protein associated with calcium-dependent chloride channel activity. *Science* 322(5901):590–594.
5. Schroeder BC, Cheng T, Jan YN, Jan LY (2008) Expression cloning of TMEM16A as a calcium-activated chloride channel subunit. *Cell* 134(6):1019–1029.
6. Stephan AB, et al. (2009) ANO2 is the cilial calcium-activated chloride channel that may mediate olfactory amplification. *Proc Natl Acad Sci USA* 106(28):11776–11781.
7. Qu Z, Hartzell HC (2000) Anion permeation in $Ca^{2+}$-activated $Cl^-$ channels. *J Gen Physiol* 116(6):825–844.
8. Ishiguro H, et al. (2009) CFTR functions as a bicarbonate channel in pancreatic duct cells. *J Gen Physiol* 133(3):315–326.
9. Sohma Y, Gray MA, Imai Y, Argent BE (2000) $HCO_3^-$ transport in a mathematical model of the pancreatic ductal epithelium. *J Membr Biol* 176(1):77–100.
10. Wang XF, et al. (2003) Involvement of CFTR in uterine bicarbonate secretion and the fertilizing capacity of sperm. *Nat Cell Biol* 5(10):902–906.
11. Lee MG, Ohana E, Park HW, Yang D, Muallem S (2012) Molecular mechanism of pancreatic and salivary gland fluid and $HCO_3$ secretion. *Physiol Rev* 92(1):39–74.
12. Hatefi Y, Hanstein WG (1969) Solubilization of particulate proteins and nonelectrolytes by chaotropic agents. *Proc Natl Acad Sci USA* 62(4):1129–1136.
13. Quinton PM (2008) Cystic fibrosis: Impaired bicarbonate secretion and mucoviscidosis. *Lancet* 372(9636):415–417.
14. Gee HY, Noh SH, Tang BL, Kim KH, Lee MG (2011) Rescue of ΔF508-CFTR trafficking via a GRASP-dependent unconventional secretion pathway. *Cell* 146(5):746–760.
15. Evans MG, Marty A (1986) Calcium-dependent chloride currents in isolated cells from rat lacrimal glands. *J Physiol* 378:437–460.
16. Nilius B, et al. (1997) Kinetic and pharmacological properties of the calcium-activated chloride-current in macrovascular endothelial cells. *Cell Calcium* 22(1):53–63.
17. Kuruma A, Hartzell HC (2000) Bimodal control of a $Ca^{2+}$-activated $Cl^-$ channel by different $Ca^{2+}$ signals. *J Gen Physiol* 115(1):59–80.
18. Namkung W, Phuan PW, Verkman AS (2011) TMEM16A inhibitors reveal TMEM16A as a minor component of calcium-activated chloride channel conductance in airway and intestinal epithelial cells. *J Biol Chem* 286(3):2365–2374.
19. Park HW, et al. (2010) Dynamic regulation of CFTR bicarbonate permeability by $[Cl^-]_i$ and its role in pancreatic bicarbonate secretion. *Gastroenterology* 139(2):620–631.
20. Smith SS, Steinle ED, Meyerhoff ME, Dawson DC (1999) Cystic fibrosis transmembrane conductance regulator. Physical basis for lyotropic anion selectivity patterns. *J Gen Physiol* 114(6):799–818.
21. Born M (1920) Volumen un hydrationwärme der ionen. *Z Phys* 1(1):45–48.
22. Suh BC, Hille B (2008) PIP2 is a necessary cofactor for ion channel function: How and why? *Annu Rev Biophys* 37:175–195.
23. Ohya Y, Botstein D (1994) Diverse essential functions revealed by complementing yeast calmodulin mutants. *Science* 263(5149):963–966.
24. Rhoads AR, Friedberg F (1997) Sequence motifs for calmodulin recognition. *FASEB J* 11(5):331–340.
25. Swindells MB, Ikura M (1996) Pre-formation of the semi-open conformation by the apo-calmodulin C-terminal domain and implications binding IQ-motifs. *Nat Struct Biol* 3(6):501–504.
26. Persechini A, Moncrief ND, Kretsinger RH (1989) The EF-hand family of calcium-modulated proteins. *Trends Neurosci* 12(11):462–467.
27. Xiao Q, et al. (2011) Voltage- and calcium-dependent gating of TMEM16A/Ano1 chloride channels are physically coupled by the first intracellular loop. *Proc Natl Acad Sci USA* 108(21):8891–8896.
28. Ferrera L, et al. (2009) Regulation of TMEM16A chloride channel properties by alternative splicing. *J Biol Chem* 284(48):33360–33368.
29. Tian Y, et al. (2011) Calmodulin-dependent activation of the epithelial calcium-dependent chloride channel TMEM16A. *FASEB J* 25(3):1058–1068.
30. Sagheddu C, et al. (2010) Calcium concentration jumps reveal dynamic ion selectivity of calcium-activated chloride currents in mouse olfactory sensory neurons and TMEM16b-transfected HEK 293T cells. *J Physiol* 588(Pt 21):4189–4204.
31. Quinton PM (2010) Role of epithelial $HCO_3^-$ transport in mucin secretion: Lessons from cystic fibrosis. *Am J Physiol Cell Physiol* 299(6):C1222–C1233.
32. Thaysen JH, Thorn NA, Schwartz IL (1954) Excretion of sodium, potassium, chloride and carbon dioxide in human parotid saliva. *Am J Physiol* 178(1):155–159.
33. Zhang GH, Cragoe EJ, Jr., Melvin JE (1992) Regulation of cytoplasmic pH in rat sublingual mucous acini at rest and during muscarinic stimulation. *J Membr Biol* 129(3):311–321.
34. Neyraud E, Bult JH, Dransfield E (2009) Continuous analysis of parotid saliva during resting and short-duration simulated chewing. *Arch Oral Biol* 54(5):449–456.
35. Lee MG, et al. (1997) Polarized expression of $Ca^{2+}$ channels in pancreatic and salivary gland cells. Correlation with initiation and propagation of $[Ca^{2+}]_i$ waves. *J Biol Chem* 272(25):15765–15770.
36. Low JT, Shukla A, Behrendorff N, Thorn P (2010) Exocytosis, dependent on $Ca^{2+}$ release from $Ca^{2+}$ stores, is regulated by $Ca^{2+}$ microdomains. *J Cell Sci* 123(Pt 18): 3201–3208.
37. Thul R, Falcke M (2004) Release currents of $IP_3$ receptor channel clusters and concentration profiles. *Biophys J* 86(5):2660–2673.